# RSC Advances

**ROYAL SOCIETY OF CHEMISTRY**

www.rsc.org/advances

**Formation of Self-assembled Multi-layer Stable Palladium Nanoparticle for Ligand-free Coupling Reactions**

Mitsuhiro Arisawa[1,2]*, Mohammad Al-Amin[1], Tetsuo Honma[3], Yusuke Tamenori[3], Satoshi Arai[4], Naoyuki Hoshiya[1], Takatoshi Sato[1], Mami Yokoyama[5], Akira Ishii[5], Masaki Takeguchi[6], Tsuyoshi Miyazaki[6], Masashi Takeuchi[4], Tomohiro Maruko[4], Satoshi Shuto[1]

[1] Faculty of Pharmaceutical Sciences, Hokkaido University, Kita-12, Nishi-6, Kita-ku, Sapporo 060-0812, Japan. [2] Graduate School of Pharmaceutical Sciences, Osaka University, Yamada-oka 1-6, Suita, Osaka 565-0871, Japan. [3] Japan Synchrotron Radiation Research Institute, 1-1-1 Kouto, Sayo-cho, Sayo-gun, Hyogo 679-5198, Japan. [4] Furuya Metal Company Limited, Minami-otsuka 2-37-5, Toshima-ku, Tokyo 170-0005, Japan. [5] Graduate School of Engineering, Tottori University, 101, Minami 4-chome, Koyama-cho, Tottori 680-8550, Japan. [6] National Institute for Materials Science, Address: 1-2-1 Sengen, Tsukuba 305-0047, Japan

**Abstract**

A structure of recently developed Pd catalyst, named sulfur-modified gold supported palladium (SAPd), has been revealed to be multi-layered Pd nanoparticle. SAPd is easily prepared by self-assembling on a sulfur-modified gold surface, and Near-edge X-ray absorption fine structure (NEXAFS) analysis at Pd K-edge determined that Pd in SAPd is zero-valence analogous to metallic Pd. On the other hand, transmission electron microscopy (TEM) analyses and extended X-ray absorption fine structure (EXAFS) analysis clarified that SAPd has approximately 10 layers of multi-layered structure and consists of nanoparticles with a diameter less than 5 nm. High-density Pd nanoparticles were embedded without

condensation. NEXAFS analysis at S and C K-edge exhibits that the organic matters

containing sulfate and xylene as a major ingredient are distributed between Pd nanoparticles

and it seems to prevent the condensation. These findings suggest that highly efficient cross

coupling reaction, which were reported in earlier works, has been achieved by the

high-density Pd nanoparticles.

1. **Introduction**

Cross-coupling reactions with an organometallic catalyst are a key for the synthesis

of functional molecules such as pharmaceuticals, agricultural chemicals, solar cells, and

organic electroluminescent displays. Especially, palladium-based catalysts show remarkable

performance owing to their high efficiency. For example, palladium-catalyzed cross-coupling

reactions are a very reliable and useful method for constructing carbon-carbon bonds of

semi-conductor monomers, pharmaceuticals, and agro chemicals[1]. For the synthesis of

functional molecules, carbon-nitrogen bond-forming reactions are useful and frequently used,

as well as carbon-carbon bond forming reactions[2, 3].

Metal cross-coupling reactions generally require the use of an excellent ligand[4, 5].

Cross-coupling reactions of metals, including these Pd-coupling reactions, have evolved with

ligand development. The ligand has several important roles in cross-coupling reactions. For

example, in the Buchwald-Hartwig reaction, the ligand acts to inhibit metal aggregation,

accelerate oxidative addition, and/or reduce elimination steps[6]. The use of ligands is, however,

associated with some problems, purification of the products. Separation of the product and

ligand is costly and takes time, and sophisticated ligands are generally expensive.

Furthermore, phosphorous ligands are easily oxidized and inert reaction conditions are generally required.

In order to emancipate cross-coupling reactions from the restrictions by the ligand, metal nanoparticles as catalysts have emerged as one of the most promising solutions. Transition metal nanoparticles are usually smaller (1–10 nm in diameter) with narrow size dispersion, and their synthesis is reproducible with a well-defined composition and clean surfaces. To achieve the useful nanoparticle catalysis, the key issue in metal nanoparticle preparation is their stabilization by a protective agent to avoid the formation of bulk metal. Two types of stabilization can be achieved depending on the nature of the protecting agents: (a) electrostatic stabilization can be achieved using ionic compounds as protecting agents; (b) steric stabilization can be achieved using neutral molecules such as polymers or other bulky molecules.[7, 8] On the other hand, the immobilization of nanoparticles on supports can increase the stability of metal dispersions and novel properties of these catalytic systems could be observed. In other words, combination of the advantages of heterogeneous and homogeneous catalysis is desirable, and the systems of organometallic catalyst involving metallic nanoparticles are an active research field.

Here we show the structural and chemical properties of recently developed novel Pd catalyst, named sulfur-modified gold supported palladium (SAPd).[9] We have characterized the structural and chemical properties of SAPd by spectroscopic analytical techniques. Extended X-ray absorption fine structure (EXAFS) experiments and transmission electron microscopy (TEM) analyses were performed to clarify the geometrical properties of Pd catalysis in SAPd. X-ray absorption near-edge structure (XANES) analysis[10] at sulfur and

carbon K-edge were used to determine the chemical states of sulfur and carbon in SAPd. As a resulrt, we found SAPd is constructed with about 10 layers of less than 5 nm Pd(0) nanoparticles.

## 2. Brief review on SAPd, sulfur-modified gold supported palladium [9]

SAPd could be easily prepared by treatment with Piranha solution, a mixture of sulfuric acid and hydrogen peroxide, and subsequent palladium absorption. In earlier investigations, SAPd has been applied to ligand-free Buchwald-Hartwig reaction and Suzuki-Miyaura couplings and carbon ($sp^3$ and $sp^2$)-hydrogen bond activation reaction, and delivered superior performance compared with conventional Pd catalysis. SAPd is an environmentally sustainable ideal catalyst, since SAPd could be usually used repeatedly and the leached Pd in the whole reaction mixture is less than 1 ppm. Now SAPd is commercially available and widely used for ligand-free Pd cross-coupling including liquid-phase combinatorial synthesis, medicinal library synthesis and flow-reaction system. Despite its high performance, several uncertainties, such as the structural and chemical properties, are still remaining.

## 3. Experiment

### 3.1; Synthesis method of SAPd

SAPd was prepared by the previously reported method[9a], which had sufficient catalytic activity on Suzuki-Miyaura coupling and Buchwald-Hartwig reaction as already reported[9a, c].

4

### 3.2; TEM analysis

The TEM grid with the foil was transferred to a JEOL JEM-ARM200F© transmission electron microscope equipped with probe-forming and imaging optics aberration correctors operated at 200 kV. Transmitted electron images were acquired by bright field (BF) and high angle annular dark field (HAADF) scanning transmission electron microscopy (STEM). STEM-Electron energy loss spectroscopy (EELS) was performed using Gatan Enfina1000© attached to the bottom of the microscope. The relevant instrument settings used during image acquisition and EELS analysis are given in Table 1.

A layer of carbon was applied to the sample surface and then platinum was FIB-deposited by injection of an organo-metallic gas and then rastering the 30kV gallium ion beam over the area of interest. A thin cross section measuring approximately 25 μ long, 2 μ wide and 8 μ deep was extracted from the die surface using a proprietary in-situ FIB technique. The cross section was attached to a 200 mesh copper TEM grid using FIB-deposited platinum. One electron transparent window was thinned to electron transparency using the gallium ion beam of the FEI FIB.

### 3.3; XAFS experiments using hard X-ray

The X-ray absorption fine structure (XAFS) measurements were performed at hard X-ray beamline BL14B2 of SPring-8 in Japan.[11] The incident hard X-rays were obtained using a silicon double crystal monochromator. The net plane is (311) for the Pd K-absorption edge. The spectra of standard materials (Pd foil, PdO, $PdSO_4$, PdS and $Pd(PPh_3)_4$) were taken in the normal transmission mode.[23] The spectra of SAPd before the $10^{th}$ cycle of the optimized Suzuki-Miyaura and Buchwald-Hartwig cross couplings (SAPd before), and after the $10^{th}$ cycle of the optimized Suzuki-Miyaura (SAPd SM after) and Buchwald-Hartwig cross

couplings (SAPd BH after), crude Suzuki-Miyaura coupling product (SM product) and crude Buchwald-Hartwig product (BH product) were measured in the fluorescent X-ray yield method using a 19-elements Ge solid state detector. All the measurements were done at room temperature. The XAFS spectra were analyzed by ATHENA and ARTEMIS XAFS analysis package.[12,13]

**3.4; XAFS experiments using soft X-ray**

The chemical state of sulfur was analyzed by using b-branch of BL27SU. The radiation from the undulator was mohochromatized by using a double crystal Si(111) monochromator ensures an energy resolution of 0.35 eV. Photon flux on the sample is $1 \times 10^{11}$ Ph/s at 2.5keV (sulfur K-edge). XANES spectra of SAPd and standard materials were recorded by partial-fluorescence yield (PFY) method by using a silicon drift detector (SDD)[14]. The chemical analysis of carbon in SAPd has been carried out at c-branch of BL27SU. At this branch, the photon beam was dispersed by a soft X-ray monochromator with varied-line-spacing plane gratings. The higher harmonics of the incident X-rays were reduced using three Cr-coated plane mirrors. The photon energy resolution during the measurements was set at 50 meV. Photon flux on the sample is $1 \times 10^{11}$ Ph/s at 0.3keV (carbon K-edge). To analyse carbon XANES spectra, palylene-N and acetic acid palladium(II) were chosen as a standard material. Palylene-N is a polymer of the *p*-xylene which is used in Pd adsorption process. All of the spectra were measured by total electron yield method. In order to eliminate the artifacts appearing in XANES spectra due to the carbon contamination of optical elements, the correct intensity curve of the incoming photon (*I0*) was measured by using Si-PIN photodiode detector after the XANES measurement of samples. SAPd samples were fixed onto a sample holder by screws, and powdered standard materials were fixed on the sample

holder by double sided carbon tape.

## 4. Results and Discussion

### 4.1; Distribution and structure of Pd in SAPd

Geometrical features of Pd in SAPd were observed by TEM analysis. Fig. 2(a) indicates a cross section of SAPd observed by TEM. The top and bottom layer corresponds to the Pt /C protection layer and Au substrate, respectively. For surface protection, whole SAPd was covered by carbon and platinum tape during TEM analysis. We observed approximately 60 to 70 nm of layers of nano-scale dots on the gold surface, which corresponds to SAPd. In Fig2(b), we can confirm nanoparticles (~5nm) embedded in SAPd. The nanoparticle observed in SAPd can be assigned to Pd nanoparticle from the scanning TEM - electron energy loss spectroscopy (STEM-EELS, Fig. 2(c)(d)) analysis. The two-dimensional elemental mapping image [Fig. 3(c)] clearly shows that the distribution of nanoparticles in Fig 3(a) coincides to the distribution of Pd. On the other hand the distribution of carbon [Fig. 2(d)] is negatively correlated to the distribution of nanoparticles observed in Fig. 3(a). This result suggests that the carbon is one of the composition elements holding Pd nanoparticles in a stable condition. TEM analysis unambiguously indicates that SAPd consists of Pd nanoparticle embedded in some matrix.

Fig. 3(a) shows enlarged view of TEM image of cross-section. The image indicates that the nanoparticles are rounded and crystalline with a diameter of about 5 nm. Fig. 3(b) exhibits the particle size distribution observed by TEM analysis. The average diameter of the nanoparicle is determined to be 4.8 nm. Particle size distribution was also determined by the

EXAFS analysis. Fig. 4(a) shows Pd K-edge $k^3\chi(k)$ EXAFS oscillations spectra of SAPd before, SAPd SM (Suzuki-Miyaura coupling)/BH (Buchwald-Hartwig reaction) after and SM/BH products and Pd foil. It is found that the amplitude of the EXAFS oscillation spectra of SAPds and SM/BH products are small compared to that of Pd foil, while the periods and the phases of the oscillations are almost same with that of Pd foil.[23] These results suggest that metallic Pd particle on SAPds and in SM/BH products is nanoparticle. Fig. 4(b) shows Pd-K edge Fourier transforms of $k^3\chi(k)$ EXAFS oscillations spectra in the $k$ range of 2.0 – 10.5 Å^{-1} of SAPds, SM product and Pd foil.[23] Fourier transforms of EXAFS oscillation spectra in the $k$ range of 2.0 – 6.5 Å^{-1} of Pd foil, SAPd before and BH product are shown inset of Fig. 4(b). To precisely investigate the size of the metallic Pd particles, theoretical curve fittings of EXAFS oscillations were performed for Pd-Pd peak in Fourier transformed the wave number $k$ space for the $k$ and radial distance $R$ ranges of 2 – 10.5 Å^{-1} and 1.75 – 3.0 Å, respectively. Only for BH product, the $k$ and $R$ ranges are 2.0 – 6.5 Å^{-1} and 2.0 – 3.4 Å, respectively. It is for this reason that the concentration of Pd in BH product is very low (< 1 ppm) and then the S/N of the EXAFS spectrum is considerably low. The parameters determined by curve fitting analysis are listed in Table 2. In the case of SAPd before, the curve fitting analysis revealed the average CN of 8.6±0.9, which is smaller than that of Pd foil. Then the average size of Pd nanoparticle with a CN of 8.6±0.9 is estimated to be about 2-4 nm.[15, 16] From the average CNs for SAPds SM/BH after and SM/BH products, the average sizes of Pd nanoparticles are estimated to be also about 2-4 nm.

The TEM and EXAFS analysis provides consistent results. EXAFS measurements at Pd K-edge region suggest that Pd atoms accumulate inside the SAPd and the mean size of the Pd nanoparticles is estimated to be 2-4 nm. Although the mean size of the Pd

nanoparticles estimated by EXAFS analysis was slightly smaller than that obtained by TEM, likely due to the difficulty in finding small Pd nanoparticles (< 1 nm) by TEM, the consistent results obtained from two independent analyses led us conclude that the Pd in SAPd is accumutated and forms nanoparticles that are less than 5 nm in size. TEM and EXAFS analysis clarified the high performance of SAPd on SM and BH reactions from the structural points of view.

The present analysis clarified that one of the novel and significant properties of SAPd is that it keeps the Pd nanoparticles stably with high density. Metal nanoparticles are the active research field since they have characteristic chemical and physical properties differing considerably from that of the bulk materials. However, the control of nanoparticle size still remains a challenge because of their high reactivity tend to form larger metal particle by condensation. The present results suggest that treatment of Au surface by Piranha solution produces the effective matrix to make Pd nanoparticles without condensation.

**4.2; Chemical analysis of Pd nanoculuster in SAPd by XANES measurement**

The next step was to determine the chemical properties of palladium content in the SAPd during the cross-coupling reactions. We measured the Pd K-edge X-ray absorption near edge structure (XANES) of SAPds before and after the 10th cycle of the optimized Pd cross-couplings and standard samples, *i.e.,* Pd foil, PdO, PdSO$_4$, PdS, and Pd(PPh$_3$)$_4$ (Fig. 5(a)).[23] The Pd K-edge XANES spectra of the SAPds before and after the 10th cycle were the same and were analogous to that of the Pd foil. These findings indicated that the Pd species of SAPds before and after use in the 10th cycle of the amination reactions were the same, and the Pd on SAPd seems to be zero-valence Pd or metallic Pd. Pd K-edge XANES

and EXAFS analyses confirmed that the Pd nanoparticles keeps 2 - 4 nm size before and after the cross-coupling reactions.

It is noteworthy that the XAFS spectra of the crude Suzuki-Miyaura coupling product and the crude Buchwald-Hartwig product were almost same as that of SAPd itself (Figs. 4 and 5(b)). Those spectra of SAPds SM/BH after and SM/BH products are identical to that of SAPd before. This analysis indicates that Pd nanoparticles in SAPd are stable and resistive against coupling reactions. Thus, SAPd achieves high reactivity and repeatability in some Pd coupling reactions without the addition of any ligands. It is concluded that the chemical state and local structure of Pd on SAPd do not change after the cross couplings and the states of Pd that remained in the product is also the same. It is concluded that the active materials are metallic Pd nanoparticles.

**4.3; Chemical analysis of matrixes in SAPd**

Figure 6 shows sulfur K-edge XANES spectra of AuS (top), SAPd (the second from top) and standard materials. [23] The XANES spectrum of SAPd indicates clear resonance peak at 2481.5 eV. On the other hand, a clear structure cannot be seen at the low energy side. The comparison with the XANES spectra of standard materials suggest that the sulfur contained in SAPd is strongly oxidized and they have the formula of $SO_4^{2-}$. The XANES spectrum of AuS is almost identical with that of SAPd, and it also shows strong $SO_4^{2-}$ resonance peak. However, we couldn't detect the sulfur signal from Au mesh which has not processed the Pirania treatment. This result indicates that the sulfur contained in SAPd is deposited by Pirania treatment and the chemical form of the adhering sulfur did not change during the following SAPd formation reaction. We can conclude that the origin of sulfur is

10

$SO_4^{2-}$ contained in the sulfuric acid used by Pirania treatment.

XANES spectra of standard material containing $SO_4^{2-}$ are indicated by blue curve. Although both $PdSO_4$ and protamine sulfate include $SO_4^{2-}$ ion, these materials show clearly different spectral profiles. Whereas protamine sulfate shows single resonance peak at 2481.5 eV, $PdSO_4$ shows small peak at about 2478.0eV. The shoulder peak was interpreted by the hybridization of S 3p states with the 3d states of the metal cation [17, 18]. XANES spectrum of SAPd does not indicate shoulder peak, and spectrum resembles to that of protamine sulfate. The present results suggest that the sulfate and palladium is not present in the form of "$PdSO_4$". This is consistent with the results of EXAFS and TEM analysis. Sulfate could interact closely with the organic matters in SAPd.

Figure 7 shows the C K-edge XANES spectra of SAPd and standard materials.[23] Top spectrum shows XANES spectrum of SAPd, and bottom spectra show the XANES spectra of standard materials. These standard specimens are the primary materials of SAPd, as was described above. Peak assignments are made by comparison with previous XANES studies of corresponding materials[19,20], and the assignments are shown in the Figure. Remarkable feature can be found at about 285.0 eV. It is well known that this peak appears in the C K-edge XANES spectra of graphite where carbon atoms has sp2 hybridization and out-of-plane π bonds, but not in that of diamond with only sp3 hybridization [21]. Therefore, the peaks at 285 eV are due to the electronic transition from C 1s to π* orbital and is a measure of the presence of conjugated bond in aromatic ring. On the other hand, the spectral features are independent of the angle between the polarization vectors of incident X-ray beam [21]. The independence suggests that the aromatic rings are randomly oriented in SAPd sample. When we discuss about the carbon chemical state based on the primary materials of SAPd,

one conceivable model is that the aromatic rings have phenyl structure and connected by $CH_2$ groups. The phenyl rings could be produced by *p*-xylene which is a solvent of a Pd nano-cluster formation. This interpretation can be supported from the experimental fact that XANES spectrum of SAPd is resembled to that of palylene-N. The origin of aromatic ring is expected to be prepared from the *p*-xylene.

Although XANES spectrum of SAPd and palylne-N are similar, there are two clear differences. First is that the $\pi^*$ excitation peak at 285 eV of palylne-N shows double peak structure. On the other hand, the intensity of higher peak is slightly suppressed in the spectrum of SAPd. It is well known that the resonance energy and peak shape of the $\pi^*$ excitation depends on the other neighbors of the excited carbon atoms. For example, when all carbon atoms in aromatic ring are equivalent, e.g., benzene, the XANES spectrum shows single resonance peak at around 285 eV [22]. On the other hand, carbon atom with a certain functional group indicates the shift of resonance energy and the resonance peak split into several peaks. Judging from these knowledges, whereas the higher energy peak originates from the excitation of carbon atom on the phenyl rings connected by $CH_2$, carbon atoms having less interaction with neighboring atoms around the aromatic ring show lower energy peak. The suppression of higher energy peak intensity suggests that the chain length of aggregated xylene is shorter than pure palylene-N polymer. The second difference is that the peak at 288.0eV is enhanced than that of palylene-N. This enhancement can be interpreted by the existence of carbonyl group in SAPd. In the SAPd synthesis processes, Pd atom is added by acetic acid palladium(II). The bottom spectrum of S6 is the XANES spectrum of acetic acid palladium(II), and we can confirm $\pi^*$(C=O) resonance peak at 288.0eV.

When we discuss about the carbon atoms in SAPd based on the primary materials

of SAPd, one conceivable model is that the xylene forms a chain of phenyl rings connected by $CH_2$ and/or $CH_3COO$, and it constructs the bone structure of SAPd. The phenyl rings could be produced by *p*-xylene which is a solvent of a Pd nano-cluster formation, and carbonyl groups could be produced by acetic acid palladium(II). The structure of SAPd implicated by the present analysis is illustrated in Fig. 8.

**4.4; Proposed structural model of SAPd**

The structure of SAPd clarified by the present analysis is indicated in Fig. 8. Two independent experiments using TEM and XAFS analysis provided complementary information. The effective catalysts in SAPd are the Pd nanoparticles, which allow for high chemical transformations due to their large surface area. An especially interesting finding was that the Pd nanoparticles are very crowded. The conventional nanoparticles used in carbon-carbon coupling reactions are usually formed by a metal salt reduction and are generally stabilized by polymeric molecules, tetraalkylammonium salt, and ionic liquids.[7, 8] The use of an appropriate stabilizing agent is therefore critical not only to obtain nanoparticles of a suitable size to form highly active catalysts, but also to stabilize the surface so that leaching is minimized and nanoparticle aggregations are prevented[19-22]. Therefore, the above results are important toward the assertion that sulfur-modified gold provides another example of an appropriate support for self-assembled multi-layers of Pd nanoparticles (less than 5 nm) in high density.

Recently, we confirmed that when we used SAPd, Suzuki-Miyaura coupling and Buchwald-Hartwig reaction proceed without any ligand[3]. The leached Pd in the whole reaction mixture is less than 1 ppm. Low-leaching is one of a significant property of SAPd.

Throughout these studies, we can see the intrinsic relationship between performance and structure.[24] That is to say, one essential property achieving the low-leaching is that Pd-nanoparticles are implanted into the sulfur-modified gold and tightly bonded. Therefore, SAPd releases only trace amounts, less than 1 ppm. On the other hand, high reactivity can be provided by active Pd nanoparticles, which are eliminated from the surface of SAPd during the reaction. This fact was confirmed based on the EXAFS measurements at the Pd K-edge, indicating that the Pd species on SAPd and the released Pd from SAPd are identical in the Suzuki-Miyaura and Buchwald-Hartwig reactions. "Sulfur-modification on gold" is a brand new and environmentally sustainable nanoparticule stabilization metod and shows the advantages of both heterogeneous and homogeneous catalysis.

## Summary

In summary, we discovered that SAPd, which catalyze Pd cross-coupling in the absence of any ligand, has approximately 10 layers of self-assembled Pd(0) nanoparticles, less than 5 nm in size, on a sulfur-modified gold surface by using XAFS and TEM analysis. It is noteworthy that the Pd nanoparticles in SAPd are embedded with high density without condensation. The matrix of SAPd, which is the organic matter formed by the complex of sulfate and xylene, embedding the Pd nanoparticle in SAPd prevent the aggregation of nanoparticle. These findings also clarify the ease and usefulness of the SAPd preparative method for constructing multi-layers of highly reactive Pd nanoparticles on metal substrates and opens a new route to prepare other metal nanoparticles for organic synthesis.

## Acknowledgement

## References

1. Yin, L.; Liebscher. J. *Chem. Rev.* **2007**, *107*, 133-173.

2. (a) Guram, A. S.; Rennels, R. A.; Buchwald. S. L. *Angew. Chem. Int. Ed.* **1995**, *34*, 1348-1350. (b) Louie, J.; Hartwig. J. F. *Tetrahedron Lett*. **1995**, *36*, 3609-3612.

3. Reviews (a) Lundgren, R. J.; Stradiotto, M. *Aldrichimica Acta* **2012**, *45*, 59-65. (b) Valente, C.; Calimsiz, S.; Hoi, K. H.; Mallik, D.; Sayah, M.; Organ, M. *Angew. Chem. Int. Ed.* **2012**, *51*, 3314-3332.

4. Martin, R.; Buchwald. S. L. *Acc. Chem. Res.* **2008**, *41*, 1461–1473.

5. Hartwig, J. F. *Acc. Chem. Res.* **2008***, 41*, 1534–1544.

6. Hartwig J. F. *Organotransition Metal Chemistry*. University Science Books, **2010**.

7. Deraedt, C.; Astruc, D. *Acc. Chem. Res.* **2014**, *47*, 494–503.

8. (a) Balanta, A.; Godard, C.; Claver, C. *Chem. Soc. Rev.* **2011**, *40*, 4973-4985. (b) Chinchilla, R.; Nájera, C. *Chem. Soc. Rev*. **2011**, *40*, 5084–5121. (c) Fihri, A.; Bouhrara, M.; Nekoueishahraki, B.; Basset, J-M. *Chem. Soc. Rev.* **2011**, *40*, 5181–5203.

9.   (a) Hoshiya, N.; Shimoda, M.; Yoshikawa, H.; Yamashita, Y.; Shuto, S.; Arisawa, M. *J. Am. Chem. Soc.* **2010**, *132*, 7270–7272. (b) Hoshiya, N.; Shuto, S.; Arisawa. M. *Adv. Synth.*

*Catal.* **2011**, *353*, 743 – 748. (c) Al-Amin, M.; Honma, T.; Hoshiya, N.; Sato, T.; Shuto, S.; Arisawa, M. *Adv. Synth. Catal.* **2012**, *354*, 1061-1068. (d) Al-Amin, M.; Arai, S.; Hoshiya, N.; Honma, T.; Tamenori, Y.; Sato, T.; Yokoyama, M.; Ishii, A.; Takeuchi, M.; Maruko, T.; Shuto, S.; Arisawa, M. *J. Org. Chem.* **2013**, *78*, 7575-7581. (e) Al-Amin, M.; Akimoto, M.; Tameno, T.; Ohki, Y.; Takahashi, N.; Hoshiya, N.; Shuto, S.; Arisawa, M. *Green Chem.* **2013**, *15*, 1142-1145. (f) Arisawa, M.; Sato, T.; Hoshiya, N.; Al-Amin, M.; Kogami, Y.; Shuto, S. *ACS Combi. Sci.* **2014,** *16*, 215-220. (g) Al-Amin, M.; Arisawa, M.; Shuto, S.; Ano, Y.; Tobisu, M.; Chatani, N. *Adv. Synth. Catal.* **2014**, *356*, 1631-1637. h) Takagi, K.; Al-Amin, M.; Hoshiya, N.; Wouters, J.; Sugimoto, H.; Shiro, Y.; Fukuda, H.; Shuto, S.; Arisawa, M. *J. Org. Chem.* **2014**, 79, 6366-6371. We made SAPd accidentally. We originally used Piranha solution just to clean up Au surface.

10. Stöhr, J.; "NEXAFS Spectroscopy" (Springer, Berlin, 1992).

11. Honma, T.; Oji, H.; Hirayama, S.; Taniguchi, Y.; Ofuchi, H.; Takagaki, M. *AIP Conf. Proc.* **2010**, *1234*, 13-16.

12. Ravel, B.; Newville, M. *J. Synchrotron Rad.* **2005**, *12*, 537-541.

13. Zabinsky, S. I.; Rehr, J. J.; Ankudinov, A. L.; Albers, R. C.; Eller, M. *J. Phys. Rev. B* **1995**, 52, 2995-3009.

14. Tamenori, Y.; Morita M.; Nakamura, T. *J. Synchrotron Rad.* **2011**, *18*, 747-752.

15. Fritsche, H. G.; Benfield, R. E. *Z. Phys. D* **1993**, *26*, 15-27.

16. Menacherry, P. V.; Garcia, M. F.; Haller, G. L. *J. Catal.* **1997**, 166, 75-88

17. Okude, N.; Nagoshi, M.; Noro, H.; Baba, Y.; Yamamoto H.; Sasaki, T. A. *J. Electron Spectr. Related. Phonomena.* **1999**, *101-103*, 607.

18. Flett, M. E.*Can. Mineral*, **2005**, *13***,** 1811.

19. Ma, Y.; Yang, H.; Guo, J.; Sathe, C.; Agui A.; Nordgren, J. *App. Phys. Lett.* **1998**, *72*, 3353.

20. Watts, B.; Swaraj, S.; Nordlund, D.; Lüning J.; Ade, H. *J. Chem. Phys.* **2011**, *134*, 024702.

21. Rosenberg, R. A.; Love, P. J.; Rehn, V. *Phys. Rev.* **1986***, B33*, 4034.

22. Kolczewski, C.; Püttner, R.; Martins, M.; Schlachter, A. S.; Snell, G.; Sant'Anna, M. M.; Hermann K.; Kaindl, G. *J. Chem. Phys.* **2006**, *124*, 014302.

23. We employed variety of standard samples as control and picked up some typical ones.

24. Until now we cannot explain the intrinsic relationship between structure and synthesis process.

**Fig. 1**. Preparation of SAPd and its use in ligand-free Pd coupling.
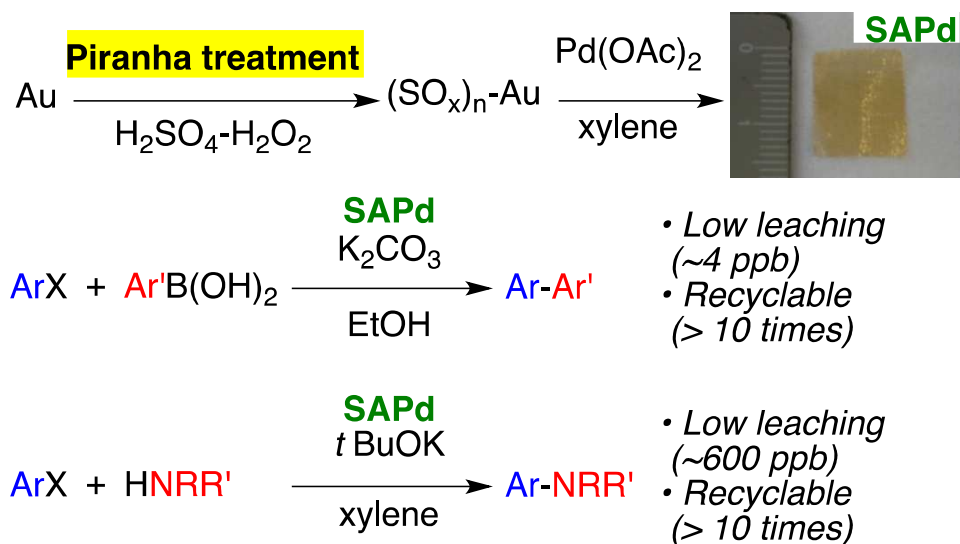
**Table 1**. Instrument Settings for imaging system used on sample.

| Instrument | transmission electron microscope |
|---|---|
| Manufacture/Model | JEOL JEM-ARM200F |
| Accelerating Voltage | 200kV |
| Condenser Aperture | 40μmφ |
| Objective Aperture | Not used |
| Objective Lens Current | Unknown |

**Table 2.** EXAFS fit parameters for Pd—Pd. Intrinsic loss factor, $S_0^2 = 0.84$ (Pd—Pd from Pd foil data).

| | CN[a] | $R$[Å][b] | $\delta^2$[Å$^2$][c] | $E_0$[eV][d] | R$_{factor}$[e] |
|---|---|---|---|---|---|
| Pd foil | 12[f] | 2.74±0.01 | 0.0056±0.0005 | -0.3±0.6 | 0.001 |
| SAPd before | 8.6±0.9 | 2.79±0.01 | 0.0075±0.0007 | -0.4±0.8 | 0.003 |
| SAPd SM after | 9.4±1.4 | 2.79±0.01 | 0.0078±0.0010 | -1.6±1.1 | 0.005 |
| SAPd BH after | 7.4±1.1 | 2.80±0.01 | 0.0076±0.0010 | -0.9±1.1 | 0.005 |
| SM product | 9.5±0.5 | 2.80±0.01 | 0.0075[g] | -2.4±1.2 | 0.010 |
| BH product | 8.1±1.7 | 2.83±0.07 | 0.0075[g] | -2.5±4.7 | 0.036 |

[a] First shell coordination number. [b] Interatomic distance. [c] Debye-Waller factor. [d] Correction of edge energy. [e] Goodness-of-fit index. [f] Coordination number was fixed as that of a fcc lattice. [g] Debye-Waller factor was fixed with the same value as the one of SAPd before.

**Fig. 2**. (a); Brightfield TEM image showing the nanoparticle-containing layer on Au. (b); enlarged view showing that the nanoparticles are rounded and crystalline. (c) and (d); Elemental mapping image of Palladium and carbon obtained by two-dimensional mapping of STEM-EELS.
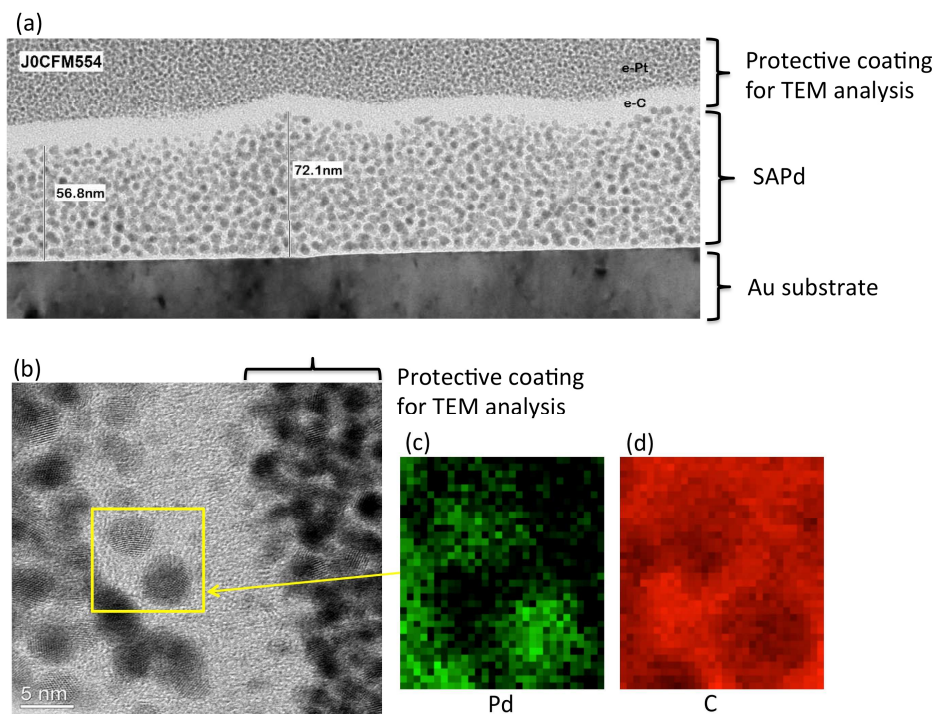
**Fig. 3**. (a) Enlarged view of cross section of SAPd. The picture shows that the nanoparticles

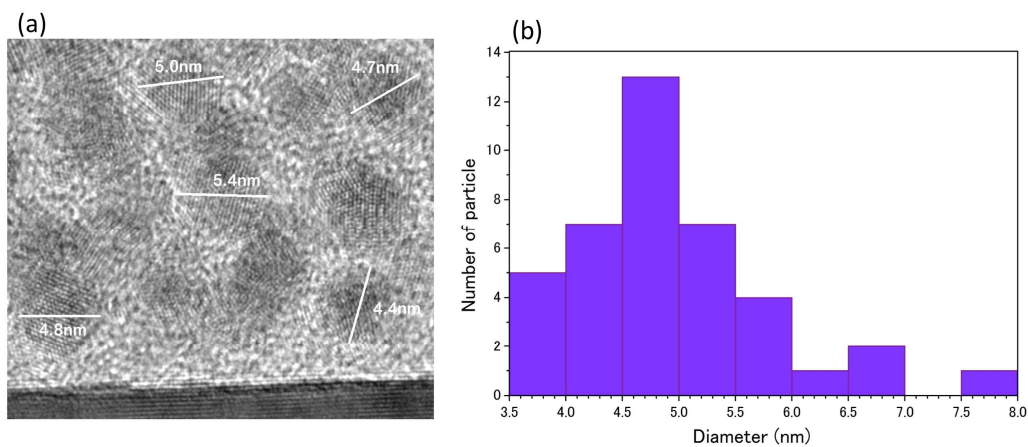are rounded and crystalline. (b) Size distribution of Pd nanoparticles obtained by TEM

analysis.

**Fig. 4** (a) Pd K-edge $k^3\chi(k)$ EXAFS oscillations spectra of SAPds and Pd foil. (b) Pd-K edge Fourier transforms of $k^3\chi(k)$ EXAFS oscillations spectra in the $k$ range of $2.0 - 10.5$ Å$^{-1}$ of SAPds, SM product and Pd foil. The inset shows Fourier transforms of EXAFS oscillation spectra in the $k$ range of $2.0 - 6.5$ Å$^{-1}$ of Pd foil, SAPd before and BH product.

23

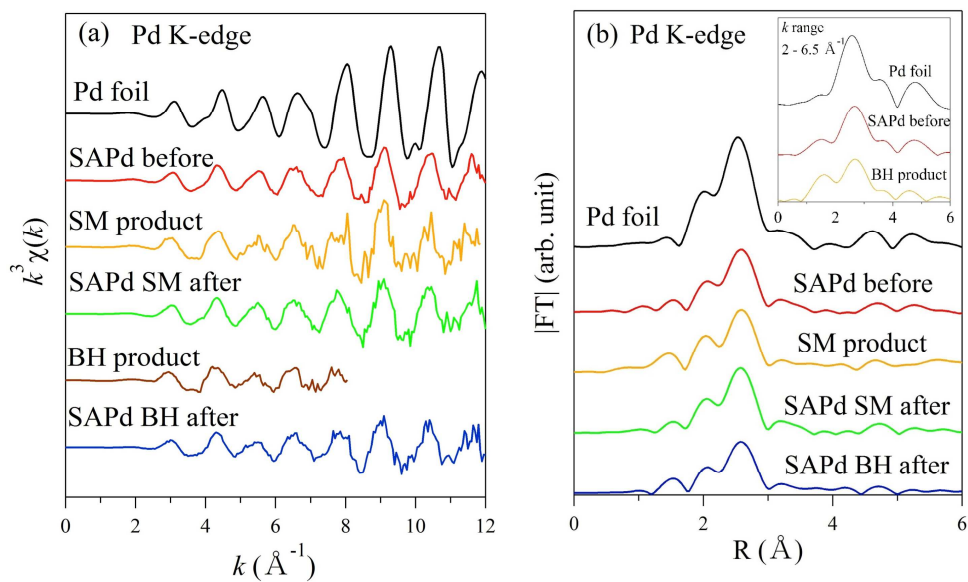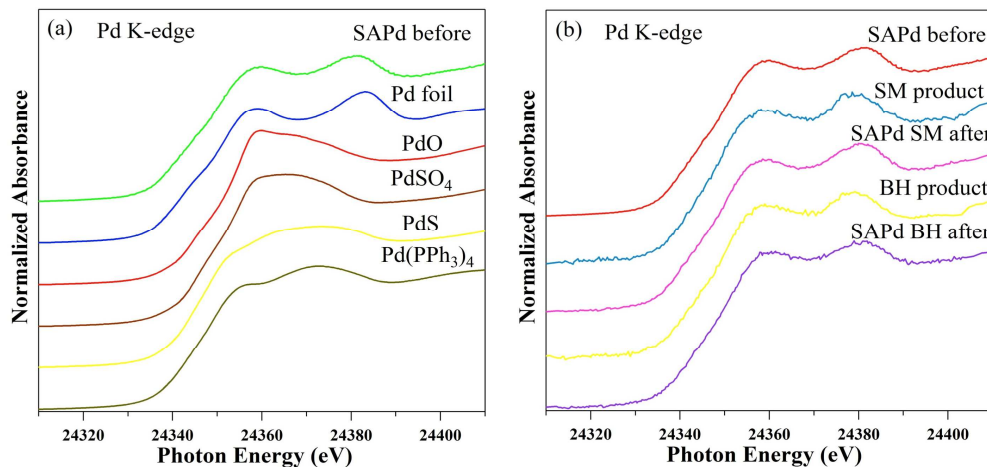**Fig. 5**. Pd K-edge XANES spectra of (a) SAPd before and standard materials, (b) SAPds.

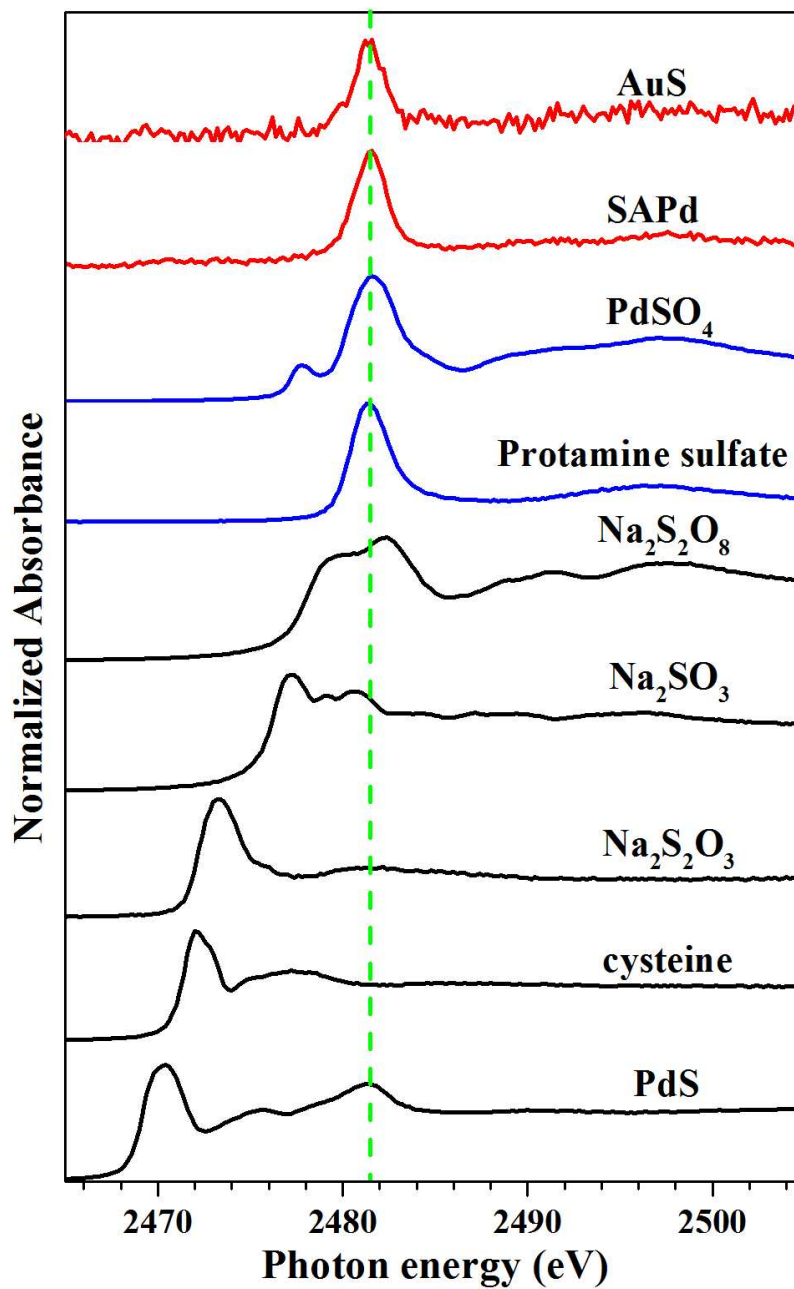**Fig. 6**. S K-edge XANES spectra of SAPd before and standard materials.

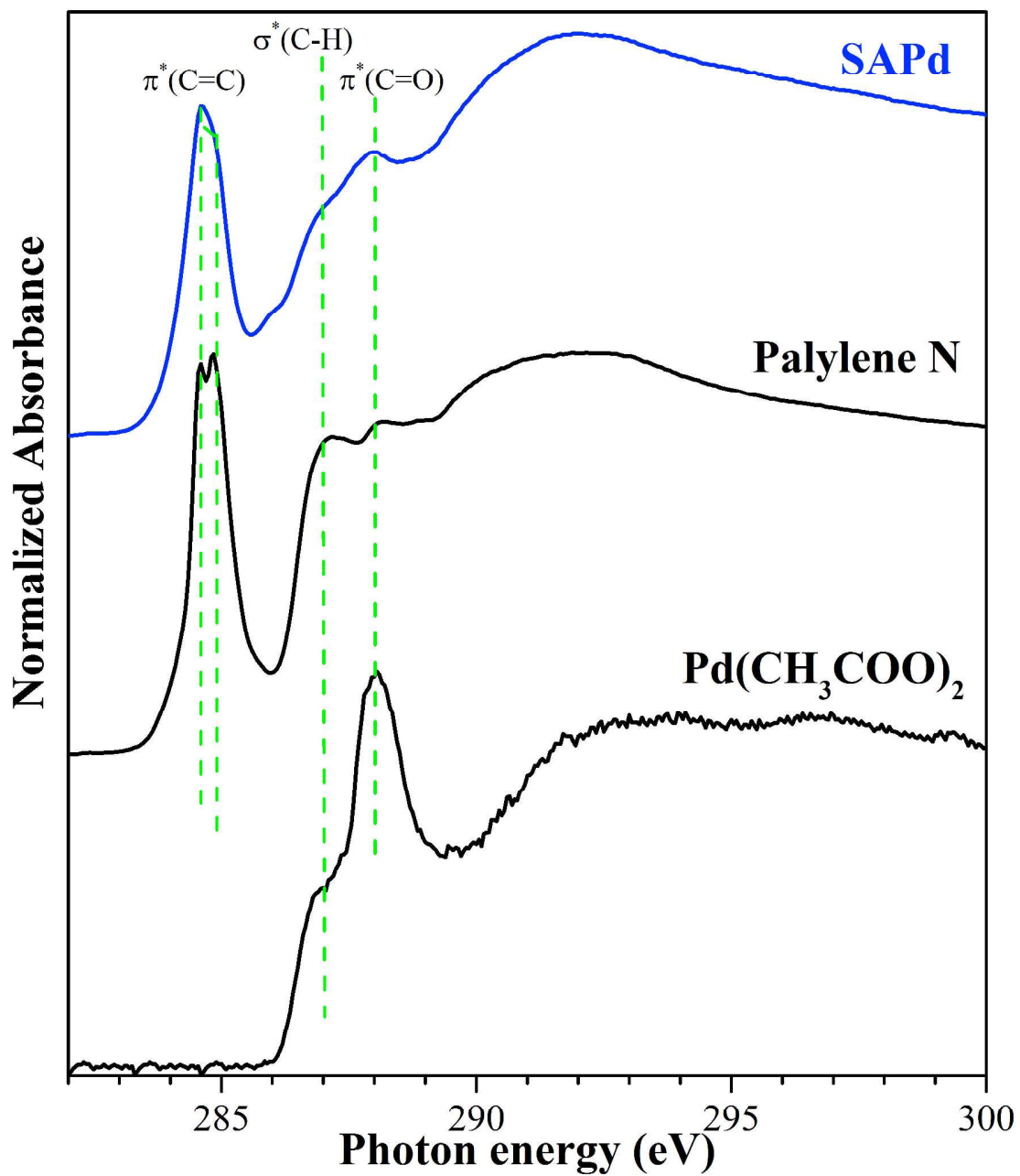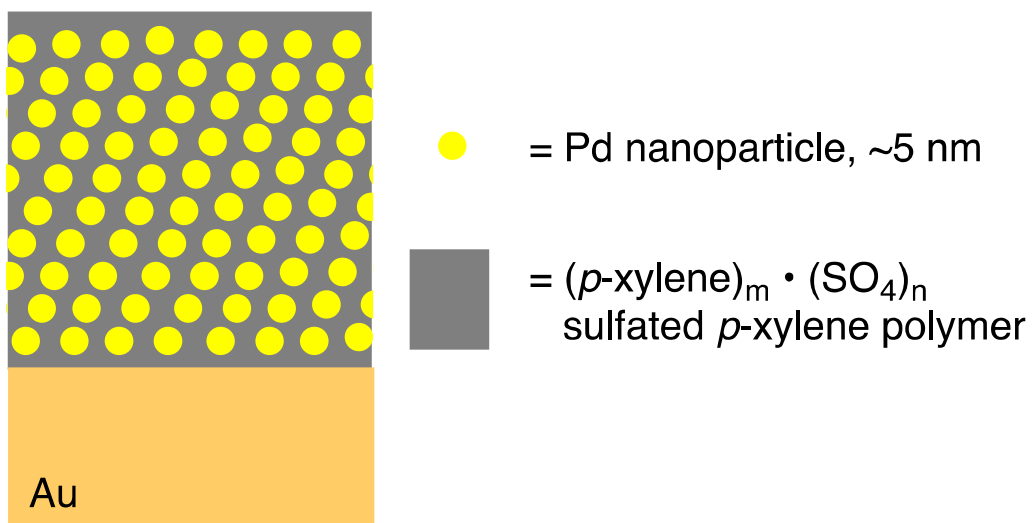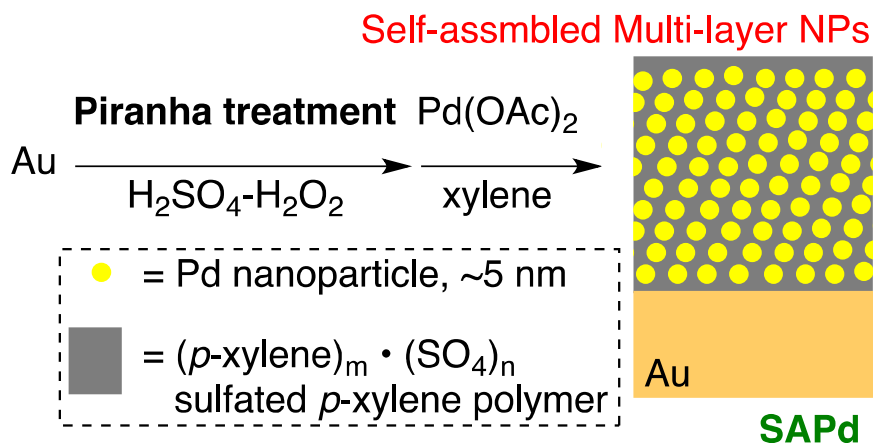**Fig. 7**. C K-edge XANES spectra of SAPd before and standard materials.

**Fig. 8**. Drawing of the SAPd structure.



● = Pd nanoparticle, ~5 nm

■ = $(p\text{-xylene})_m \cdot (SO_4)_n$
  sulfated $p$-xylene polymer

Au

Self-assmbled Multi-layer NPs

**Piranha treatment** Pd(OAc)$_2$

Au $\xrightarrow[\text{H}_2\text{SO}_4\text{-H}_2\text{O}_2]{}$ $\xrightarrow[\text{xylene}]{}$

● = Pd nanoparticle, ~5 nm

■ = ($p$-xylene)$_m$ • (SO$_4$)$_n$ sulfated $p$-xylene polymer

Au

**SAPd**

**SAPd** works for ligand-free Buchwald-Hartwig reaction and Suzuki-Miyaura coupling with low-leaching (< 1 ppm) and high recyclability (>10 times).

RSC Advances Accepted Manuscript